Impact of Attractive Interactions on the Rheology of Dense Athermal Particles

Ehsan Irani,[1] Pinaki Chaudhuri,[2] and Claus Heussinger[1]
[1]Institute for Theoretical Physics, Georg-August University of Göttingen, Friedrich-Hund Platz 1, 37077 Göttingen, Germany
[2]Institut für Theoretische Physik II, Heinrich-Heine-Universität Düsseldorf, 40225 Düsseldorf, Germany
(Received 20 December 2013; published 9 May 2014)

Using numerical simulations, the rheological response of an athermal assembly of soft particles with tunable attractive interactions is studied in the vicinity of jamming. At small attractions, a fragile solid develops and a finite yield stress is measured. Moreover, the measured flow curves have unstable regimes, which lead to persistent shear banding. These features are rationalized by establishing a link between the rheology and the interparticle connectivity, which also provides a minimal model to describe the flow curves.

DOI: 10.1103/PhysRevLett.112.188303 PACS numbers: 83.60.Wc, 66.20.Cy, 83.10.Rs, 83.50.-v

In nature, soft disordered solids occur in different forms (e.g., gels, emulsions, colloids, foams, grains, etc.) across a wide range of packing fractions ϕ, which are made possible by the tuning of particle interactions. The flow properties of these soft materials have been harnessed for various applications, e.g., in the food or chemical industries. Thus, understanding the role of particle interactions and the corresponding mechanisms which lead to observed rheological behavior is an important recurrent theme.

For non-Brownian suspensions of frictionless repulsive spheres, it is observed that ramping up the packing fraction results in the occurrence of jamming at $\phi = \phi_J$ [1,2]. The rheological signature of the onset of jamming is the development of a finite yield stress at ϕ_J [3]. For Brownian suspensions of such particles, it has been shown that a yield stress exists at $\phi < \phi_J$, due to the presence of thermal vibrations [4]. A similar systematic investigation of how the jamming paradigm is changing upon the introduction of attractive particle interactions is still missing. It is known that at smaller ϕ, such systems do exhibit finite yield stress [5–8], but a quantitative bridge with the jamming scenario needs to be developed.

Such studies are also needed since shear banding, the phenomenon of spatially inhomogeneous flows observed in many soft yield-stress fluids [9,10], has often been attributed to attractive interactions [6,11]. In general, persistent occurrence of shear bands has been linked to nonmonotonic constitutive laws leading to flow instabilities [9,12] (e.g., in micelles [13]). It is not known how interparticle attractions could result in such instabilities.

Conceptually, one can imagine the steady flowing state to be a regime where there is a continuous competition between the rupturing induced by shear and processes that try to restore local structure. Theoretical models suggest that nonmonotonic flow curves can occur due to long-lived local fluidizations when the post-rupture restructuring takes a very long time [14–16]. However, experiments and numerical simulations have shown that for $\phi > \phi_J$, no such instabilities occur in the flow curve for either repulsive or attractive systems [17–20]. The question now arises whether, for $\phi < \phi_J$, a short-ranged attraction which introduces a new length scale for structure formation leads to longer restoration time scales and if this is, indeed, the origin of a shear banding instability.

In this Letter, we report a simulational study of the variation in rheological behavior of an athermal assembly of soft disks, near ϕ_J, by the tuning up of attractive interactions. We show that, for $\phi < \phi_J$, minimal attractions result in finite yield stresses. The variation of this threshold with attraction and packing fractions can be rationalized in terms of changing structure, viz. the number of contacts per particle and its link with isostaticity. Further, we demonstrate for the first time the existence of nonmonotonic flow curves at these weak attractions, causing persistent shear banding over a range of shear rates. Thus, our work reveals new rheological behavior in the vicinity of ϕ_J with the introduction of attractive interactions and demonstrates how the flow properties gradually deviate from that of repulsive particles.

In our numerical simulations (using LAMMPS [21]), we study a two-dimensional 50:50 binary mixture of soft disks, having a size ratio of 1.4. The disks interact via the following potential, which can be considered to be a model for cohesive grains or attractive emulsions [7,20]

$$V(r_{ij}) = \begin{cases} \epsilon\left[\left(1-\frac{r_{ij}}{d_{ij}}\right)^2 - 2u^2\right], & \frac{r_{ij}}{d_{ij}} < 1+u, \\ -\epsilon\left[1+2u-\frac{r_{ij}}{d_{ij}}\right]^2, & 1+u < \frac{r_{ij}}{d_{ij}} < 1+2u, \\ 0, & \frac{r_{ij}}{d_{ij}} > 1+2u, \end{cases} \tag{1}$$

where $d_{ij} = (d_i + d_j)/2$, and d_i being the diameter of disk i. Such a potential results in piecewise-linear interaction forces. The strength and the range of the attractive forces

are simultaneously tuned by varying u (see inset of Fig. 2 for a schematic). We shear the system of particles at any imposed shear rate $\dot{\gamma}$ by using the appropriate Lees-Edwards boundary conditions. During the flow, when two particles overlap, they experience a dissipative force which depends on their relative velocity: $-b[(\vec{v}_i - \vec{v}_j).\hat{r}_{ij}]\hat{r}_{ij}$, where b is the damping coefficient, and $\hat{r}_{ij}$ is the unit vector between particles i and j. We integrate the corresponding Newton's equations of motion for different system sizes $N = 10^3$, 10^4, 2×10^4 in order to explore the rheological properties for a wide range of packing fractions ϕ. In our simulations, the units for energy, length, and time are, respectively, ϵ, d_s, and $\sqrt{md_s^2/\epsilon}$, where m is the mass of the particles and d_s is the diameter of the smaller particles. Further, by our choices of $m = 1$, $\epsilon = 1$, $b = 2$, particles undergo overdamped dynamics via inelastic collisions [22,23].

First, we focus on how the flow curves (σ vs $\dot{\gamma}$) shape up after the attractive interactions are introduced. In Fig. 1(a), for a system size of $N = 10^3$, we show the flow curves at $\phi = 0.82$ (which is less than $\phi_J \approx 0.843$). For the purely repulsive system ($u = 0$), we observe the usual Bagnold scaling $\sigma \sim \dot{\gamma}^2$ [23]. As soon as the attraction strength is finite, the particle assembly exhibits a finite (albeit small) yield stress σ_y. The yield stress increases with increasing attraction, which is expected. We also note that at larger $\dot{\gamma}$, the flow curves for all attraction strengths collapse and are identical to the repulsive case. Thus, attraction has an effect only at small shear rates and the range over which this change occurs increases with increasing attraction strength. We will call these two regimes "attraction-dominated" and "repulsion-dominated" flow in the following.

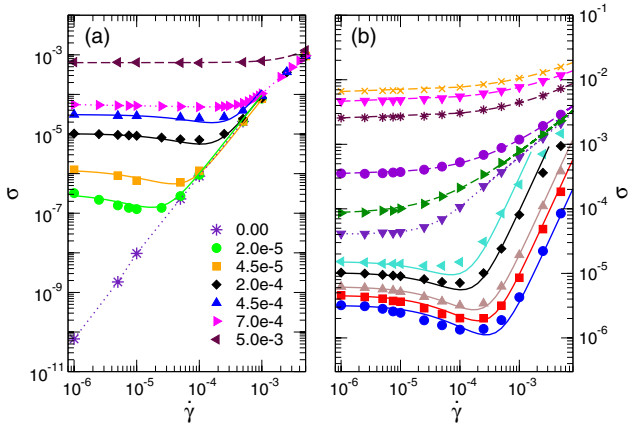

FIG. 1 (color online). Shear stress σ as a function of strain rate $\dot{\gamma}$ for $N = 10^3$: (a) for different attraction strengths u (as specified in the legends) at $\phi = 0.82$; (b) for different packing fractions (from the bottom to top) $\phi = 0.75$, 0.78, 0.80, 0.82, 0.83, 0.84, 0.843, 0.85, 0.9, 0.95, 1.0 for the attraction strength $u = 2 \times 10^{-4}$. The solid lines are fits using the fluidity model [Eq. (3)], the dashed lines are Herschel-Bulkley fits, and the dotted lines are guides to the eye.

In Fig. 1(b), we show the variation of the flow curves with packing fraction ϕ for a fixed $u = 2 \times 10^{-4}$. We observe that the system exhibits a finite σ_y at ϕ much below $\phi_J(\approx 0.843)$. At $\phi > \phi_J$, we observe the usual Herschel-Bulkley form, consistent with previous work [20].

In both panels of Fig. 1, the flow curves are visibly nonmonotonic, for either (a) low attraction strengths or (b) low packing fractions. In both cases, there exists an intermediate regime of shear rates, where shear stress is a decreasing function of strain rate $\dot{\gamma}$. As discussed earlier, such flow curves lead to localized shear bands; i.e., homogeneous flow is no longer possible.

It is known that under imposed $\dot{\gamma}$, shear band formation can be avoided if the wavelengths of the unstable modes do not fit into the lateral size of the simulation box [24]. Thus, in our simulations, for a system size of $N = 10^3$ (data in Figs. 1–4), velocity profiles measured in the unstable regime of the flow curve are seen to be linear, i.e., homogeneous flow is observed. However, when the system size is increased to $N = 10^4$, 2×10^4, the rapid formation of permanent shear bands, in this regime, is observed. Further, in this unstable part, when stress-controlled simulations are done, we observe either runaway flow towards the stable high-shear rate branch or absorption into an arrested state [25].

With the minimum in the flow curve being quite shallow, the tendency to form shear bands in our system is weak. This gives us a rare opportunity to study not only the properties and formation of shear bands, but also the underlying, nominally unstable, constitutive law.

By gathering data for different ϕ and u, we look at the variation of the yield stress, $\sigma_y \equiv \sigma(\dot{\gamma} \to 0)$, which is estimated from the stress at the smallest available strain rate ($\dot{\gamma} = 10^{-6}$ or 10^{-7}); this is shown in Fig. 2. For high volume fractions ϕ and small attraction strength u—in the

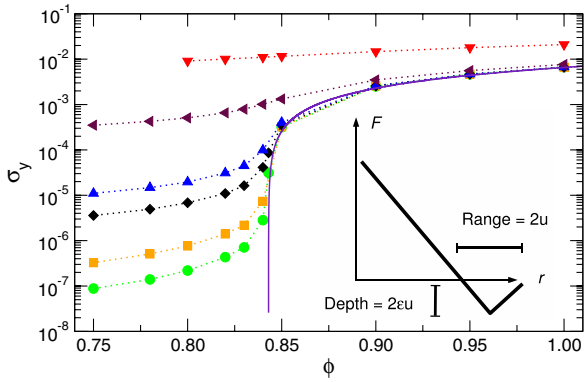

FIG. 2 (color online). Variation of yield stress σ_y with packing fraction ϕ for different attraction strengths (from bottom to top) $u = 2 \times 10^{-5}$, 4.5×10^{-5}, 2×10^{-4}, 4.5×10^{-4}, 5×10^{-3}, 5×10^{-2}. Solid line: yield stress of the repulsive system ($u \to 0$) is expected to vanish at $\phi = \phi_J$ as $\sigma_y^{(\mathrm{rep})} \propto (\phi - \phi_J)^{\alpha}$; $\alpha = 1.04$. (Inset): schematic of the particle interaction force $F(r)$.

repulsion-dominated regime—the yield stress is independent of u and scales as $\sigma_y^{(\mathrm{rep})} \propto (\phi - \phi_J)^{\alpha}$. The fitted value of the exponent $\alpha \approx 1.04$ is consistent with previous results for purely repulsive particles [3], but likely suffers from finite-size effects [26]. For strong attraction, the yield stress is only weakly density dependent and scales linearly with the strength of attraction, i.e., $\sigma_y \sim u$. Such a property is trivially expected from the rupture of a single element of strength u.

The new and nontrivial result is the regime at small u and below the jamming limit ($\phi < \phi_J$). There, a finite yield stress is observed even at densities nominally far below ϕ_J, where the corresponding repulsive system is a normal fluid. Thus, in weakly attractive systems, the crossover from attraction-dominated to repulsion-dominated flow can also be observed by increasing ϕ. Note the similarity with the repulsive but Brownian system [4], where a crossover occurs from a "weakly thermal" regime ($\phi < \phi_J$) to an athermal regime ($\phi > \phi_J$).

What is the proper energy scale in the weakly attractive regime? In order to answer this question, we first take a look at the connectivity z, defined as the average number of contacts per particle. In counting the contact number, we include all nearest neighbors lying within the range of the interaction potential. The typical variation of z as a function of strain rate is shown in the two panels of Fig. 3 for (a) fixed ϕ and (b) fixed u; the values of the different parameters are the same as in Fig. 1.

We concentrate on small strain rates first. For the repulsive particles, $z \to 0$ at vanishing shear rates, as expected for our model of inertial, dissipative dynamics [23]. However, as soon as u is finite, $z_0 \equiv z(\dot\gamma \to 0)$ jumps to a finite value. In both panels of Fig. 3, we notice that z_0

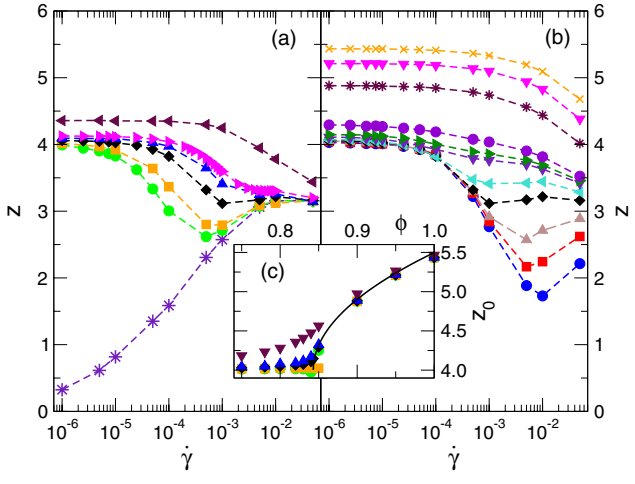

FIG. 3 (color online). Variation of coordination number z as a function of strain rate $\dot\gamma$ (a) for different attraction strengths (u) at $\phi = 0.82$ and (b) for different ϕ at a fixed $u = 2 \times 10^{-4}$. The values of u in (a) and ϕ in (b) are the same as those in Fig. 1. Dashed lines are guides to the eye. (c) Variation of $z_0 \equiv z(\dot\gamma \to 0)$ with ϕ. The solid line denotes $(\phi - \phi_J)^{1/2}$.

saturates at a value not much larger than the isostatic limit $z_{\mathrm{iso}} = 4$ as $\dot\gamma \to 0$. Thus, minimal attraction leads to similar isostatic structures as seen in the purely repulsive system for $\phi = \phi_J$. The difference being that, here, isostatic networks are observed over a range of volume fractions and considerably below ϕ_J. At high ϕ, the familiar scaling law, $z_0 - z_{\mathrm{iso}} = \zeta_0(\phi - \phi_J)^{1/2}$; $\zeta_0 \approx 3.78$ [27] is recovered [see Fig. 3(c)].

Previous work on packings of soft repulsive particles and elastic networks [1] have shown how linear elasticity in the near-isostatic regime can be understood in terms of the deviation from isostaticity, $\delta z = z_0 - z_{\mathrm{iso}}$. It turns out that we can use a similar reasoning to derive the scaling form for the yield stress in the attraction-dominated regime to be $\sigma_y^{(\mathrm{att})} \sim u^{1/2}\delta z^{3/2}$ (see Supplemental Material [25]). With this, and the repulsive yield stress $\sigma_y^{(\mathrm{rep})} \sim \delta\phi^{\alpha}\theta(\delta\phi)$, the overall yield stress can be written as follows:

$$\sigma_y/|\delta\phi|^{\alpha} \propto \begin{cases} u^{1/2}\delta z^{3/2}/|\delta\phi|^{\alpha}, & \sigma_y^{(\mathrm{rep})} \ll \sigma_y^{(\mathrm{att})}, \\ 1, & \sigma_y^{(\mathrm{rep})} \gg \sigma_y^{(\mathrm{att})}. \end{cases} \quad (2)$$

This scaling form is verified in Fig. 4(a), using the data for σ_y shown in Fig. 2 and the corresponding data for z_0. The data collapse on the two branches defined by Eq. (2) is excellent and holds over several orders of magnitude. We also note some deviations for the smallest attraction strengths and packing fractions.

We return to discussing the rheology at finite $\dot\gamma$, where a similar link exists. As with the nonmonotonic flow curves, we see a nonmonotonic behavior also in z vs $\dot\gamma$ (Fig. 3). At small strain rates, where $\sigma(\dot\gamma)$ is decreasing, $z(\dot\gamma)$ quickly drops to values far below $z_{\mathrm{iso}} = 4$, before it rises again following the repulsive branch.

Here, we see the manifestation of the two competing mechanisms described in the introduction: shear-induced rupture of the fragile near-isostatic network and attraction-induced aggregation (see the supporting movies in the Supplemental Material [25]). At small but finite $\dot\gamma$, the imposed shear is not fast enough to efficiently destroy the ever continuous restructuration. At large $\dot\gamma$, on the other hand, the intrinsic relaxation time is too large to lead to the buildup of a large aggregate.

To extract a characteristic time scale for this aggregation process, we demonstrate that by using the scaling form $z(\dot\gamma) = z_0 - \dot\gamma\tau_a$, it is possible to collapse all the data for z vs $\dot\gamma$ in the regime of weak attraction [see Fig. 4(b)]. While generating the scaling collapse, we obtain $\tau_a \approx 0.5/u$, for the intrinsic time scale for restructuration. Thus, for weak attractions, τ_a is large. Now, for shear banding to occur, applied shear rates need to satisfy $\dot\gamma\tau_a < 1$. Hence, shear banding can only be observed in the regime of small u, which agrees with the flow curves of Fig. 1.

Moreover, we can use the attraction-dependent time scale within a simple model to provide a reasonable fit

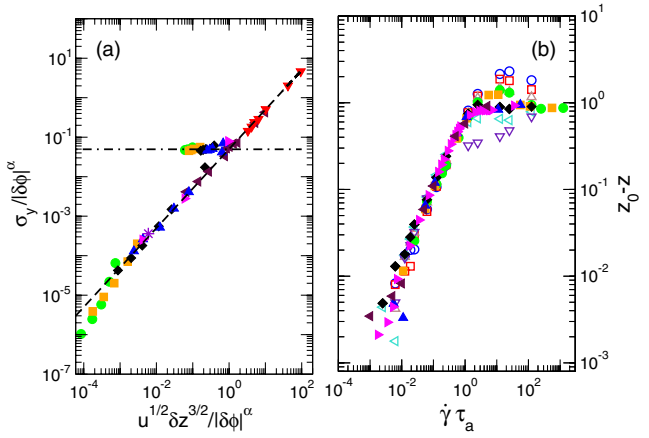

FIG. 4 (color online). Scaling plots: (a) Yield stress σ_y normalized by $|\delta\phi|^\alpha$ as a function of the combination $u^{1/2}\delta z^{3/2}|\delta\phi|^{-\alpha}$. Dashed lines correspond to the two regimes of Eq. (2). (b) Variation of $z_0 - z$ with $\dot\gamma\tau_a$ (where $\tau_a = 0.5/u$), using data shown in Fig. 3(a) (closed symbols) and Fig. 3(b) (open symbols).

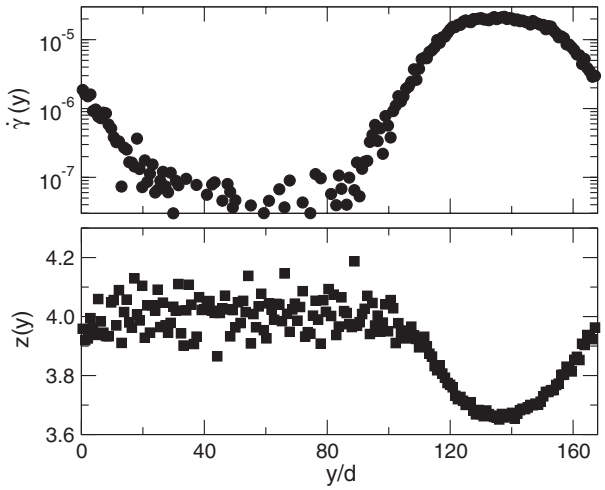

FIG. 5. At $\phi = 0.82$, $u = 2 \times 10^{-5}$ and $\dot\gamma = 5 \times 10^{-6}$: Spatial profile of (top) local shear rate $\dot\gamma(y)$ and (bottom) the corresponding local contact numbers $z(y)$ for $N = 2 \times 10^4$.

to these flow curves. Based on the fluidity approach of Picard *et al.* [28], we can derive (for details, see Supplemental Material [25]) the following simple expression for the stress:

$$\sigma(\dot\gamma) = \sigma_y^{(\mathrm{att})}\frac{W(\dot\gamma\tau)}{\dot\gamma\tau} + \sigma^{(\mathrm{rep})}(\dot\gamma). \tag{3}$$

$W(x)$ is the Lambert-W function, and the time scale is taken to inversely depend on attraction strength $\tau \sim u^{-1}$ (i.e., proportional to τ_a). The repulsive branch is assumed to show Bagnold scaling, $\sigma^{(\mathrm{rep})} \sim \dot\gamma^2$. The underlying physics of the model is the above mentioned competition between shear-induced fluidization and intrinsic relaxation or aggregation. Despite the simplicity of the model, the nonmonotonic flow curves can be fitted surprisingly well, as shown in Figs. 1(a)–1(b). Nevertheless, the model cannot reproduce some details of the simulation data: for example, the precise functional form in the limit of small $\dot\gamma$. The fluidity model (as well as others [15,16,29]) gives $\sigma \to \sigma_y/(1 + \dot\gamma\tau)$ for small $\dot\gamma$. The simulation data hint at a weaker (logarithmic) dependence on strain rate in this limit. More work is needed to resolve this issue, both from a theoretical point of view and from the simulations.

The link between connectivity and flow is further illustrated when, for a shear banded state, one measures the spatial profiles of local shear rates and the corresponding local connectivity. This is shown in Fig. 5, at a state point $\{\phi, \dot\gamma, u\}$ in the unstable regime of the flow curve [see Fig. 1(a)] for a large enough system size and measured during a long strain window. It is clear that the flowing region has a low connectivity, while the arrested band is nearly isostatic with $z \approx 4$. Future studies should address formation and properties of these shear bands.

To conclude, in the proximity of ϕ_J, we have studied how weak attractive interactions (u) change the rheological properties of dense disordered assemblies of non-Brownian particles. First, we rationalized the existence of finite yield stresses below the (repulsive) jamming transition via a scaling argument that exploits the near-isostatic nature of the contact network, viz. $\sigma_y \sim u^{1/2}(z - z_{\mathrm{iso}})^{3/2}$. Second, we demonstrated the occurrence of nonmonotonic flow curves indicating a shear banding instability. We showed that this feature is a consequence of a long structural aggregation time scale $\tau \sim u^{-1}$, which can be extracted from the loss of connectivity as the shear rate is increased. With this time scale at hand, we set up a fluidity model to provide reasonable fits to the nonmonotonic flow curves. Thus, we established how the emerging rheological changes are linked to properties of the contact network.

An expected consequence of the nonmonotonicity is that static and dynamic yield stresses will be different (as, e.g., reported in Ref. [8]). However, the inverse does not necessarily follow; i.e., a difference between static and dynamic thresholds does not necessarily imply a nonmonotonic flow curve. Thus, independent studies using imposed stress and imposed strain rate are necessary.

Future work should explore the impact of thermal fluctuations on the rheological behavior observed by us, thus, making the possible link with the flow behavior of dense gel glasses. Also, studies should be extended to lower packing fractions where more open-ended fragile networks of the attractive particles are expected to occur [7,30]. In parallel, systematic experiments are necessary at these packing fractions in order to further test our findings. While there have been recent experiments probing static properties of jammed attractive assemblies [31] or their shear moduli [32], more detailed rheological studies of these dense fragile networks are necessary.

We acknowledge financial support by the DFG via the Emmy Noether Program (No. He 6322/1-1). We also thank J. Horbach for useful discussions.

[1] M. van Hecke, J. Phys. Condens. Matter **22**, 033101 (2010).
[2] A. J. Liu, and S. Nagel, Annu. Rev. Condens. Matter Phys. **1**, 347 (2010).
[3] C. Heussinger, P. Chaudhuri, and J.-L. Barrat, Soft Matter **6**, 3050 (2010).
[4] A. Ikeda, L. Berthier, and P. Sollich, Phys. Rev. Lett. **109**, 018301 (2012).
[5] P. Coussot, Soft Matter **3**, 528 (2007).
[6] P. Moller, A. Fall, V. Chikkadi, D. Derks, and D. Bonn, Phil. Trans. R. Soc. A **367**, 5139 (2009).
[7] G. Lois, J. Blawzdziewicz, and C. S. OHern, Phys. Rev. Lett. **100**, 028001 (2008).
[8] S. H. Ebrahimnazhad Rahbari, J. Vollmer, S. Herminghaus, and M. Brinkmann, Phys. Rev. E **82**, 061305 (2010).
[9] P. Schall and M. van Hecke, Annu. Rev. Fluid Mech. **42**, 67 (2010).
[10] G. Ovarlez, S. Rodts, X. Chateau, and P. Coussot, Rheol. Acta **48**, 831 (2009).
[11] L. Bécu, S. Manneville, and A. Colin, Phys. Rev. Lett. **96**, 138302 (2006).
[12] S. M. Fielding, arXiv:1309.3422v1.
[13] L. Bécu, S. Manneville, and A. Colin, Phys. Rev. Lett. **93**, 018301 (2004).
[14] V. Mansard, A. Colin, P. Chaudhuri, and L. Bocquet, Soft Matter **7**, 5524 (2011).
[15] K. Martens, L. Bocquet, and J.-L. Barrat, Soft Matter **8**, 4197 (2012).
[16] P. Coussot and G. Ovarlez, Eur. Phys. J. E **33**, 183 (2010).
[17] G. Ovarlez, K. Krishan, and S. Cohen-Addad, Europhys. Lett. **91**, 68005 (2010).
[18] R. Besseling, L. Isa, P. Ballesta, G. Petekidis, M. E. Cates, and W. C. K. Poon, Phys. Rev. Lett. **105**, 268301 (2010).
[19] S. Mandal, M. Gross, D. Raabe, and F. Varnik, Phys. Rev. Lett. **108**, 098301 (2012).
[20] P. Chaudhuri, L. Berthier, and L. Bocquet, Phys. Rev. E **85**, 021503 (2012).
[21] http://lammps.sandia.gov/index.html.
[22] N. Xu, C. S. O'Hern, and L. Kondic, Phys. Rev. Lett. **94**, 016001 (2005).
[23] D. Vågberg, P. Olsson, and S. Teitel, arXiv:1312.5158.
[24] J. K. G. Dhont, Phys. Rev. E **60**, 4534 (1999).
[25] See Supplemental Material at http://link.aps.org/supplemental/10.1103/PhysRevLett.112.188303 for movies and details of analysis.
[26] P. Olsson and S. Teitel, Phys. Rev. E **83**, 030302 (2011).
[27] C. S. O'Hern, L. E. Silbert, A. J. Liu, and S. R. Nagel, Phys. Rev. E **68**, 011306 (2003).
[28] G. Picard, A. Ajdari, L. Bocquet, and F Lequeux, Phys. Rev. E **66**, 051501 (2002).
[29] P. D. Olmsted, Rheol. Acta **47**, 283 (2008).
[30] F. A. Gilabert, J.-N. Roux, and A. Castellanos, Phys. Rev. E **78**, 031305 (2008).
[31] I. Jorjadze, L-L. Pontani, K. A. Newhall, and J. Brujić, Proc. Natl. Acad. Sci. U.S.A. **108**, 4286 (2011).
[32] S. S. Datta, D. D. Gerrard, T. S. Rhodes, T. G. Mason, and D. A. Weitz, Phys. Rev. E **84**, 041404 (2011).